Astrophysics and Space Science
DOI 10.1007/sXXXXX-XXX-XXXX-X

GRMHD/RMHD Simulations & Stability of Magnetized Spine-Sheath Relativistic Jets

Philip Hardee [1], Yosuke Mizuno [2,3], & Ken-Ichi Nishikawa [2,4]

Abstract A new general relativistic magnetohydrodynamics (GRMHD) code "RAISHIN" used to simulate jet generation by rotating and non-rotating black holes with a geometrically thin Keplarian accretion disk finds that the jet develops a spine-sheath structure in the rotating black hole case. Spine-sheath structure and strong magnetic fields significantly modify the Kelvin-Helmholtz (KH) velocity shear driven instability. The RAISHIN code has been used in its relativistic magnetohydrodynamic (RMHD) configuration to study the effects of strong magnetic fields and weakly relativistic sheath motion, c/2, on the KH instability associated with a relativistic, $\gamma = 2.5$, jet spine-sheath interaction. In the simulations sound speeds up to ? $c/\sqrt{3}$ and Alfvén wave speeds up to ? 0.56 c are considered. Numerical simulation results are compared to theoretical predictions from a new normal mode analysis of the RMHD equations. Increased stability of a weakly magnetized system resulting from c/2 sheath speeds and stabilization of a strongly magnetized system resulting from c/2 sheath speeds is found.

Keywords galaxies: jets — gamma rays: bursts — ISM: jets and outflows — methods: analytical — MHD — relativity — instabilities

1 Introduction

Relativistic jets are associated with active galactic nuclei and quasars (AGN), with black hole binary systems (microquasars), and are thought responsible for the gamma-ray bursts (GRBs). The observed proper motions in AGN and microquasar jets imply speeds from ? 0.9 c (e.g., Mirabel & Rodriquez 1999) up to ? 0.999 c (e.g., the 3C 345 jet Zensus et al. 1995; Steffen et al. 1995), and the inferred speeds for GRBs are ? 0.99999 c (e.g., Piran 2005).

Jets at the larger scales may be kinetically dominated and contain relatively weak magnetic fields, but stronger magnetic fields exist closer to the acceleration and collimation region. Here GRMHD simulations of jet formation (e.g., Koide et al. 2000; Nishikawa et al. 2005; De Villiers et al. 2003, 2005; Hawley & Krolik 2006; McKinney & Gammie 2004; McKinney 2006; Mizuno et al. 2006) and earlier theoretical work (e.g., Lovelace 1976; Blandford 1976; Blandford & Znajek 1977; Blandford & Payne 1982) invoke strong magnetic fields. Additionally, the GRMHD simulations suggest that jets driven by magnetic fields threading the ergosphere can reside within a broader sheath outflow driven by the magnetic fields anchored in the accretion disk (e.g., McKinney 2006; Hawley & Krolik 2006; Mizuno et al. 2006), or less collimated accretion disk wind (e.g., Nishikawa et al. 2005).

Recent observations of QSO winds with speeds, ? 0.1 – 0.4c, also indicate that a jet could reside in a high speed sheath (Chartas et al. 2002, 2003; Pounds et al. 2003a, 2003b; Reeves et al. 2003). Circumstantial evidence such as the requirement for large Lorentz factors suggested by the TeV BL Lacs when contrasted with much slower observed motions has been used to suggest the presence of a spine-sheath morphology (Ghisellini et al. 2005), and Siemignowska et al. (2006) have proposed a spine-sheath model for the PKS 1127-145 jet. Spine-sheath structure has also been proposed based on theoretical arguments (e.g., Sol et al. 1989; Henri & Pelletier 1991; Laing 1996; Meier 2003) and has been investigated in the context of GRB jets (e.g., Rossi et

Philip Hardee, Yosuke Mizuno, & Ken-Ichi Nishikawa
[1] The University of Alabama (UA), Tuscaloosa, AL, 35487 USA
[2] National Space Science & Technology Center (NSSTC), Huntsville, AL 35805 USA
[3] NASA/Marshall Space Flight Center (NASA/MSFC), Huntsville, AL 35805 USA
[4] University of Alabama at Huntsville (UAH), Huntsville, AL 35805 USA

al. 2002; Lazzatti & Begelman 2005; Zhang et al. 2003, 2004; Morsony et al. 2006).

In §2 we illustrate the spine-sheath configuration found by our GRMHD jet generation simulations. Previous relativistic fluid dynamical (RHD) simulation and theoretical work has shown the importance of spine-sheath structure to KH instability (Hardee & Hughes 2003). In §3 we report on numerical results that extend this previous investigation numerically and in §4 theoretically to the strongly magnetized RMHD regime.

2 GRMHD Jet Spine-Sheath Generation

In order to study the formation of relativistic jets from a geometrically thin Keplerian disk, we use a 2.5-dimensional GRMHD code with Boyer-Lindquist coordinates (r, θ, ϕ). The method is based on a 3+1 formalism of the general relativistic conservation laws of particle number and energy momentum, Maxwell equations, and Ohm's law with no electrical resistance (ideal MHD condition) in a curved spacetime. In the simulations presented here we use minmod slope limiter reconstruction, HLL approximate Riemann solver, flux-CT scheme and Noble's 2D method (see Mizuno et al. 2006 and references therein).

A geometrically thin Keplerian disk rotates around a black hole (non-rotating, $a = 0.0$ or rapidly co-rotating, $a = 0.95$, here a is black hole spin parameter), where the disk density is 100 times the coronal density. The thickness of the disk is $H/r \sim 0.06$. The background corona is free-falling, and the initial magnetic field is uniform and parallel to the rotational axis. Simulations are normalized by the speed of light, c, and the Schwarzschild radius, r_S, with timescale, $\tau_S \equiv r_S/c$. Values of the magnetic field strength and gas pressure depend on the normalized density, ρ_0. In these simulations the magnetic field strength, B_0, is set to $0.05\sqrt{\rho_0 c^2}$). The 128 × 128 computational grid with logarithmic spacing in the radial direction spans the region $1.1r_S \leq r \leq 20.0r_S$ (non-rotating black hole) and $0.75r_S \leq r \leq 20.0r_S$ (rapidly rotating black hole) and $0.03 \leq \theta \leq \pi/2$ where we assume axisymmetry with respect to the z-axis and mirror symmetry with respect to the equatorial plane. We employ a free boundary condition at the inner and outer boundaries in the radial direction.

Figure 1 shows snapshots of the density (panels (a) and (b)), plasma beta ($\beta = p_{\rm gas}/p_{\rm mag}$) distribution (panels (c) and (d)), and total velocity (panels (e) and (f)) for the non-rotating black hole, $a = 0.0$ (left panels); and the rapidly rotating black hole, $a = 0.95$ (right panels); at each simulation's terminal time (non-rotating: $t = 275\tau_S$ and rotating: $t = 200\tau_S$). At the marginally stable circular orbit ($r = 3r_S$) the disk orbits the black hole in about $40\tau_S$. The total velocity distribution of non-rotating and rapidly rotating black hole cases are shown in Figs. 1e and 1f. The jets in both

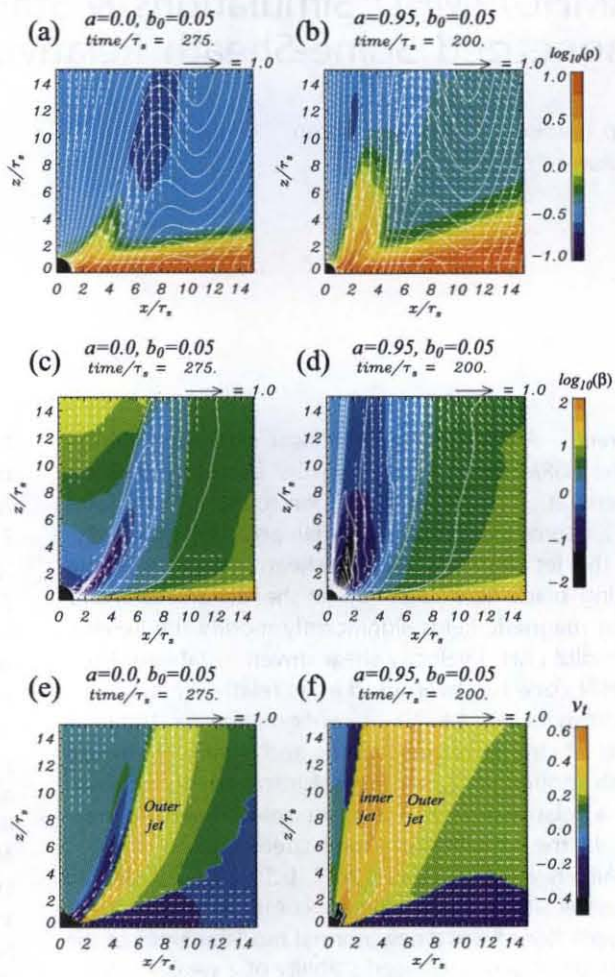

Fig. 1.— Snapshots of the non-rotating black hole (*a, c, e*) and the rapidly rotating black hole (*b, d, f*) at the applicable terminal simulation time. The color scales show the logarithm of density (upper panels), plasma beta ($\beta = p_{\rm gas}/p_{\rm mag}$; middle panels) and total velocity (lower panels). A negative velocity indicates inflow towards the black hole. The white lines indicate magnetic field lines (contour of the poloidal vector potential; upper panels) and contours of the toroidal magnetic field strength (middle panels). Arrows depict the poloidal velocities normalized to light speed, as indicated above each panel by the arrow.

cases have speeds greater than 0.4 c (mildly relativistic) that are comparable to the Alfvén speeds. In the jets, toroidal velocity is the dominant velocity component. In the rapidly rotating black hole case, the velocity distribution indicates a two-component jet with the inner jet not seen in the non-rotating black hole case. The inner jet is faster than the outer jet (over $0.5c$).

3 RMHD Spine-Sheath Simulations

In these simulations a "preexisting" jet is established across a computational domain of $6R_j \times 6R_j \times 60R_j$ with $60 \times 60 \times 600$ zones. The jet is in total pressure balance with a lower-density magnetized sheath with $\rho_j/\rho_e = 2.0$, where ρ is the mass density in the proper frame. The jet speed is $u_j = 0.9165\ c$ and $\gamma_j \equiv (1-u_j^2)^{-1/2} = 2.5$. The initial magnetic field is uniform and parallel to the jet flow. A precessional perturbation is applied at the inflow by imposing a transverse component of velocity with $u_\perp = 0.01 u_j$. Here we show simulations with a precessional perturbation of angular frequency $\omega R_j/u_j = 0.93$. In order to investigate the effect of an external wind, we have performed a no wind case ($u_e = 0$) and a relativistic wind case ($u_e = 0.5\ c$). Simulations are halted after ~ 60 light crossing times of the jet radius (see Mizuno et al. 2007 for details).

We have performed weakly magnetized simulations with sound speeds $a_e \sim 0.57\ c$ and $a_j \sim 0.51\ c$, and Alfvén speeds $v_{Ae} \sim 0.07\ c$ and $v_{Aj} \sim 0.06\ c$. The stabilizing effect of a sheath wind is revealed in Figure 2. Here we see considerable reduction in transverse structure and the jet spine reaches a larger distance before disruption in the presence of a wind.

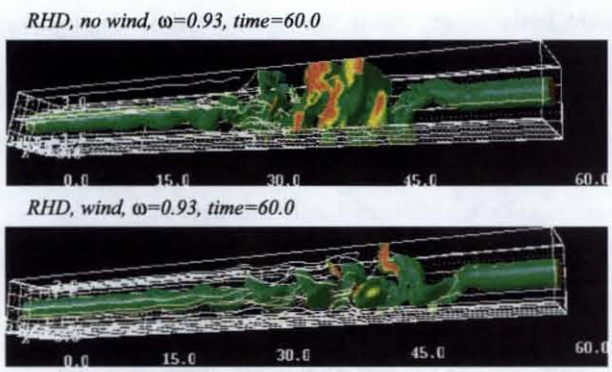

Fig. 2.— 3D isovolume density image of the weakly magnetized case with no wind (top) and a c/2 wind (bottom). Magnetic field lines in white.

We have also performed strongly magnetized simulations with Alfvén speeds $v_{Ae} \sim 0.56\ c$ and $v_{Aj} \sim 0.45\ c$, and sound speeds $a_e \sim 0.30\ c$ and $a_j \sim 0.23\ c$. The stabilizing influence of a magnetic field and the stabilization of the jet spine in the presence of a magnetized sheath wind is shown in Figure 3. Here we see that the presence of the strong magnetic field has stabilized the jet spine even more than occured for the weakly magnetized wind case and the initial helical perturbation is damped in the presence of the strongly magnetized sheath wind.

More quantitatively we can analyse the growth or damping of the initial perturbation via 1D cuts in the radial velocity as shown in Figure 4. Measurable reduction in transverse motion is seen for the weakly magnetized wind case, significant reduction occurs for the strongly magnetized no wind case and stabilization occurs in the strongly magnetized wind case.

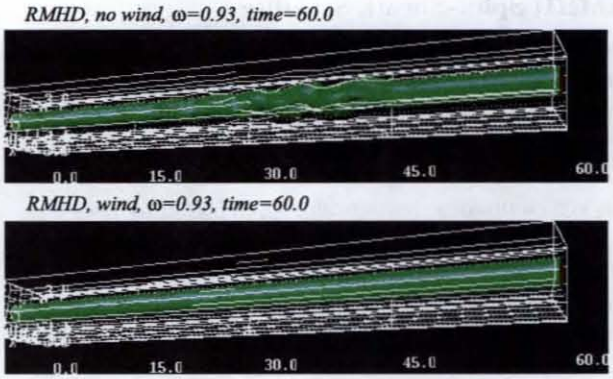

Fig. 3.— 3D isovolume density image of the strongly magnetized case with no wind (top) and a c/2 wind (bottom). Magnetic field lines in white.

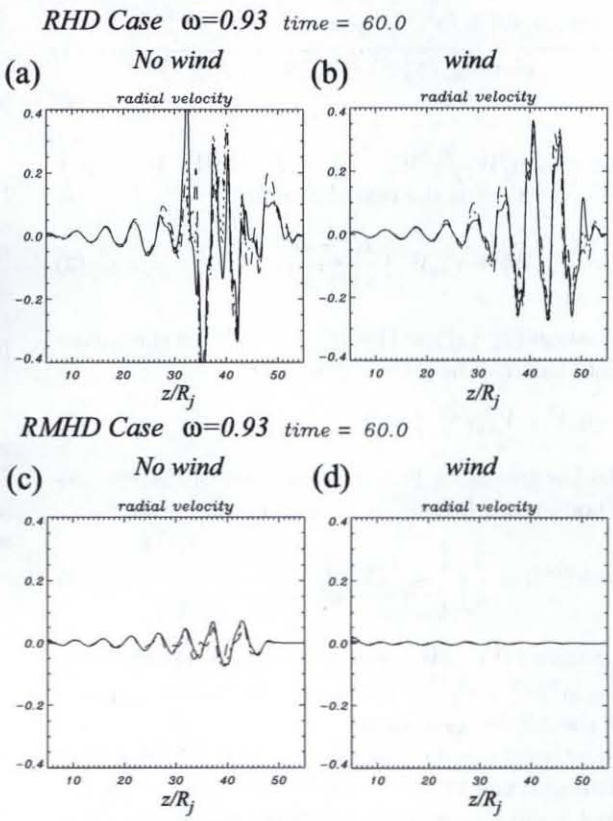

Fig. 4.— Radial velocity (v_x) along one dimensional cuts parallel to the jet axis and located at $x/R_J = 0.2$ (solid line), 0.5 (dotted line) and 0.8 (dashed line) for the weakly magnetized (top) and strongly magnetized cases (bottom).

4 RMHD Spine-Sheath Stability

Stability of a jet spine-sheath configuration can be analyzed by modeling the jet/spine as a cylinder of radius R embedded in an infinite sheath. A dispersion relation describing the growth or damping of the normal modes can be derived assuming uniform conditions within the spine, e.g., a uniform proper density, ρ_j, axial magnetic field, $B_j = B_{j,z}$, and velocity, $\mathbf{u}_j = u_{j,z}$, and assuming uniform conditions in the external sheath, e.g., a uniform proper density, ρ_e, axial magnetic field, $B_e = B_{e,z}$, and velocity $\mathbf{u}_e = u_{e,z}$ (see Hardee 2007).

Each normal mode consists of a single fundamental and multiple body wave solutions to the dispersion relation. In the low frequency limit the helical fundamental mode has an analytical solution given by

$$\frac{\omega}{k} = \frac{[\eta u_j + u_e] \pm i\eta^{1/2}\left[(u_j - u_e)^2 - V_{As}^2/\gamma_j^2\gamma_e^2\right]^{1/2}}{(1 + V_{Ae}^2/\gamma_e^2 c^2) + \eta(1 + V_{Aj}^2/\gamma_j^2 c^2)} \tag{1}$$

where $\eta \equiv \gamma_j^2 W_j / \gamma_e^2 W_e$, $V_A^2 \equiv B^2/4\pi W$, $W \equiv \rho + [\Gamma/(\Gamma - 1)] P/c^2$ is the enthalpy, and

$$V_{As}^2 \equiv \left(\gamma_{Aj}^2 W_j + \gamma_{Ae}^2 W_e\right) \frac{B_j^2 + B_e^2}{4\pi W_j W_e} \ . \tag{2}$$

In equation (2) $\gamma_{Aj,e} \equiv (1 - v_{Aj,e}^2/c^2)^{-1/2}$ is the Alfvén Lorentz factor. The jet is stable when

$$(u_j - u_e)^2 - V_{As}^2/\gamma_j^2\gamma_e^2 < 0 \ . \tag{3}$$

In the low frequency limit the real part of the first helical body mode has an analytical solution given by

$$kR \approx k^{\min} R \equiv \frac{5}{4}\pi \left[\frac{v_{msj}^2 u_j^2 - v_{Aj}^2 a_j^2}{\gamma_j^2 (u_j^2 - a_j^2)(u_j^2 - v_{Aj}^2)}\right]^{1/2} \ . \tag{4}$$

In equation (4) v_{ms} is a magnetosonic speed defined by $v_{ms} \equiv \left[a^2/\gamma_A^2 + v_A^2\right]^{1/2}$ where a is the sound speed, and v_A is the Alfvén wave speed.

Equations (1 & 4) provide estimates for the helical fundamental and first body modes that can be followed by root finding techniques to higher frequencies. The results of numerical solution to the dispersion relation for the parameters appropriate to the numerical simulations shown in §3 are displayed in Figure 5.

In the weakly magnetized cases fundamental (**S**) mode solutions consist of a growing (shown) and damped (not shown) solution pair (see eq. 1) and first body (**B1**) mode solutions consist of a real and growing or damped solution pair. The presence of the external wind flow leads to reduced growth of the S mode and weak damping of the B1 mode.

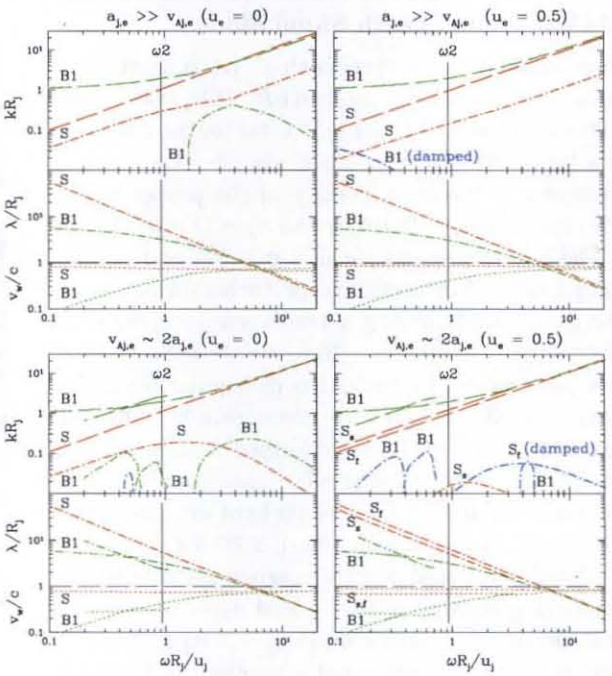

Fig. 5.— Solutions for helical fundamental (red lines) and first body (green lines) modes for weakly magnetized ($a_{j,e} \gg v_{Aj,e}$) and strongly magnetized ($v_{Aj,e} \sim 2a_{j,e}$) jet simulations with no wind ($u_e = 0$) and with a c/2 wind ($u_e = 0.5$). Solutions show the real, $k_r R_j$, (dashed lines) and imaginary, $k_i R_j$, (dash-dot lines) parts of the wavenumber as a function of the angular frequency, $\omega R_j/u_j$. Where the imaginary part of the wavenumber is shown in blue, the solution is damped. Immediately under the solutions for fundamental (**S**) and first body (**B1**) modes is a panel that shows the wavelength, λ/R_j, (dash-dot lines) and wave speed, v_w/c, (dotted lines). The simulation precession frequency $\omega 2 = 0.93$ is indicated by the vertical solid line.

In the strongly magnetized no wind case S mode solutions again consist of a growing and damped solution pair. However, we now find multiple growing solutions associated with the B1 mode at lower frequencies, and a modest damping rate accompanies the crossing of the multiple body mode solutions. At higher frequencies the B1 mode is similar to the weakly magnetized case.

In the strongly magnetized wind case weak growth is associated with the slower, S_s, moving shorter wavelength solution and weak damping is associated with the faster, S_f, moving longer wavelength solution. At frequencies, $\lesssim \omega 2$, the growth rate is larger than the damping rate but at higher frequencies the damping rate is larger than growth rate for the S mode solution pair. In general the B1 mode is damped.

5 Conclusions

Increased stability of the weakly-magnetized system with mildly relativistic sheath flow and stabilization of the strongly-magnetized system with mildly relativistic sheath flow is in agreement with theoretical results. In the fluid limit the present results confirm earlier results obtained by Hardee & Hughes (2003), who found that the development of sheath flow around a relativistic jet spine explained the partial stabilization of the jets in their numerical simulations.

The simulation results agree with theoretically predicted wavelengths and wave speeds. On the other hand, growth rates and spatial growth lengths obtained from the linearized equations or from the present relatively low resolution simulations only provide guidelines to the rate at which perturbations grow or damp.

A rapid decline in perturbation amplitudes in the sheath as a function of radius, governed by a Hankel function in the dispersion relation, suggests that the present results will apply to sheaths more than about three times the spine radius in thickness.

Where flow and magentic fields are parallel, current driven (**CD**) modes are stable (Isotomin & Pariev 1994, 1996). However, we expect magnetic fields to have a significant toroidal component. Provided radial gradients are not too large we expect the present results to remain approximately valid where $u_{j,e}$ and $B_{j,e}$ refer to poloidal velocity and magnetic field components.

In the helically twisted magnetic and flow field regime likely to be relevant to many astrophysical jets CD modes (Lyubarskii 1999) and/or KH modes could be unstable. While both CD and KH instability produce helically twisted structure, the conditions for instability, the radial structure, the growth rate and the pattern motions are different. These differences may serve to identify the source of helical structure on relativistic jet flows and allow determination of jet properties near to the central engine.

Resarch supported by NASA/MSFC cooperative agreement NCC8-256 and NSF award AST-0506666 to UA (P. Hardee), the NASA/MSFC postdoctoral program administered by ORAU (Y. Mizuno), and by NASA awards NNG-05GK73G, HST-AR-10966.01-A and NSF award AST-0506719 to UAH (K. Nishikawa). The numerical simulations were performed on the IBM p690 at NCSA and the Altix3700 BX2 at YITP.

References

Blandford, R. D. 1976, MNRAS, 176, 465
Blandford, R.D., & Payne, D.G. 1982, MNRAS, 199, 883
Blandford, R.D., & Znajek, R.L. 1977, MNRAS, 179, 433
Chartas, G., Brandt, W N., & Gallagher, S.C. 2003, ApJ, 595, 85
Chartas, G., Brandt, W.N., Gallagher, S. C., & Garmire, G.P. 2002, ApJ, 579, 169
De Villiers, J.-P., Hawley, J.F., & Krolik, J.H. 2003, ApJ, 599, 1238
De Villiers, J.-P., Hawley, J.F., Krolik, J.H., & Hirose, S. 2005, ApJ, 620, 878
Ghisellini, G., Tavecchio, F., & Chiaberge, M. 2005, A&A, 432, 401
Hardee, P.E. 2007, ApJ, submitted
Hardee, P.E., & Hughes, P.A. 2003, ApJ, 583, 116
Hawley, J.F., & Krolik, J.H. 2006, ApJ, 641, 103
Henri, G., & Pelletier, G. 1991, ApJ, 383, L7
Istomin, Y.N., & Pariev, V.I. 1994, MNRAS, 267, 629
Istomin, Y. N., & Pariev, V.I. 1996, MNRAS, 281, 1
Koide, S., Meier, D.L., Shibata, K., & Kudoh, T. 2000, ApJ, 536, 668
Laing, R. A. 2001, ASP Conf. Series 100: Energy Transport in Radio Galaxies and Quasars, eds. P.E. Hardee, A.H. Bridle & A. Zensus (San Francisco: ASP), 241
Lazzati, D., & Begelman, M.C. 2005, ApJ, 629, 903
Lovelace, R.V.E. 1976, Nature, 262, 649
Lyubarskii, Y.E. 1999, MNRAS, 308, 1006
McKinney, J.C. 2006, MNRAS, 368, 1561
McKinney, J.C. & Gammie, C.F. 2004, ApJ, 977
Meier, D.L. 2003, New A Rev., 47, 667
Mirabel, I.F., & Rodriguez, L.F. 1999, ARAA, 37, 409
Mizuno, Y., Nishikawa, K.-I., Koide, S., Hardee, P., & Fishman, G.J. 2006, PoS (http://pos.sissa.it), MQW6, 045
Mizuno, Y., Hardee, P.E., & Nishikawa, K.-I. 2007, ApJ, submitted
Morsony, B.J., Lazzati, D., & Begelman, M C. 2006, (astro-ph/0609254)
Nishikawa, K.-I., Richardson, G., Koide, S., Shibata, K., Kudoh, T., Hardee, P., & Fishman, G.J. 2005, ApJ, 625, 60
Piran, T. 2005, Rev. Mod. Phys., 76, 1143
Pounds, K.A., King, A.R., Page, K.L., & O'Brien, P.T. 2003a, MNRAS, 346, 1025
Pounds, K.A., Reeves, J.N., King, A.R., Page, K.L., O'Brien, P.T., & Turner, M.J.L. 2003b, MNRAS, 345, 705
Reeves, J.N., O'Brien, P.T., & Ward, M. J. 2003, ApJ, 593, L65
Rossi, E., Lazzati, D., & Rees, M.J. 2002, MNRAS, 332, 945
Siemiginowska, A., Stawarz, L., Cheung, C. C., Harris, D. E., Sikora, M., Aldcroft, T. L., & Bechtold, J. 2007, ApJ, in press
Sol, H., Pelletier, G., & Assero, E. 1989, MNRAS, 237, 411
Steffen, W., Zensus, J.A., Krichbaum, T.P., Witzel, A., & Qian, S.J. 1995, A&A, 302, 335
Zhang, W., Woosley, S.E., & Heger, A. 2004, ApJ, 608, 365
Zhang, W., Woosley, S.E., & MacFadyen, A. I. 2003, ApJ, 586, 356
Zensus, J. A., Cohen, M. H., & Unwin, S. C. 1995, ApJ, 443, 35

This 2-column preprint was prepared with the AAS LaTeX macros v5.2.